Current Biology 19, 2102–2107, December 29, 2009 ©2009 Elsevier Ltd All rights reserved DOI 10.1016/j.cub.2009.10.075

Report

Shape and Dynamics of Tip-Growing Cells

Otger Campàs[1] and L. Mahadevan[1,2,3,*]
[1]School of Engineering and Applied Sciences, Harvard University, 29 Oxford Street, Cambridge, MA 02138, USA
[2]Department of Organismic and Evolutionary Biology, Harvard University, 16 Divinity Avenue, Cambridge, MA 02138, USA
[3]Department of Systems Biology, Harvard Medical School, 200 Longwood Ave, Alpert 536, Boston, MA 02115, USA

Summary

Walled cells have the ability to remodel their shape while sustaining an internal turgor pressure that can reach values up to 10 atmospheres [1–7]. Although it is undisputed that this requires a tight and simultaneous regulation of cell wall assembly and mechanics, previous theoretical studies on tip growth focused either on the mechanical behavior of the cell wall or on its assembly [8–14]. To study the interplay between growth and mechanics in shaping a walled cell, we examine the particularly simple geometry of tip-growing cells [1, 3, 15, 16], which elongate via the assembly and expansion of cell wall in the apical region of the cell. We describe the observed irreversible expansion of the cell wall during growth as the extension of an inhomogeneous viscous fluid shell under the action of turgor pressure, fed by a material source in the neighborhood of the growing tip. This allows us to determine theoretically the radius of the cell and its growth velocity in terms of the turgor pressure and the secretion rate and rheology of the cell wall material. We derive simple scaling laws for the geometry of the cell and find that a single dimensionless parameter, which characterizes the relative roles of cell wall assembly and expansion, is sufficient to explain the observed variability in shapes of tip-growing cells. More generally, our description provides a framework to understand cell growth and remodeling in plants (pollen tubes [17], root hairs, etc. [18]), fungi (hyphal growth [19, 20] and fission and budding yeast [3]), and some bacteria [21], in the context of both tip growth and diffuse growth.

Theoretical Description and Results

The shape of a walled cell is specified by its cell wall. From a geometrical viewpoint, cell walls are shell-like structures [1, 6] of thickness 0.1–1 μm [6], always much thinner than the observed radii of curvature of the shell, which is of the order of 10 μm (Figure 1). Therefore, a steadily elongating tip-growing cell can be described as an axisymmetric thin shell of radius $r(s)$ and thickness $h(s)$, with s being the contour length from the apex (Figure 1C). The geometry of the shell is characterized by its principal curvatures, κ_s along the tangential direction, s, and κ_ϕ along the azimuthal direction, ϕ. Defining θ as the angle between the local normal and the direction of growth (Figure 1C), the curvatures read $\kappa_s = d\theta/ds$ and $\kappa_\phi = \sin\theta/r$. The stress resultants (tensions) σ_{ss} and $\sigma_{\phi\phi}$ in a shell subject to a pressure P (the turgor) are given by

$$\kappa_s\sigma_{ss} + \kappa_\phi\sigma_{\phi\phi} = P\,,$$

$$\kappa_\phi\sigma_{ss} = \frac{P}{2}\,, \tag{1}$$

and follow from a consideration of the balance of forces in the longitudinal and azimuthal directions, regardless of the mechanical properties of the cell wall (see Supplemental Data, available online, for details). The tensions in the cell wall must be related to the deformation rates (i.e., the expansion) of the tubular shell via the rheology of the cell wall. In order to account for the observed irreversible expansion of the cell wall in the apical region, we describe it as an inhomogeneous but locally isotropic viscous shell, with a viscosity that varies with location following the distribution of enzymes that regulate the local crosslinking state of the wall (cell wall loosening enzymes [6, 16, 22]; Pectin methylesterases (PMEs) and PME inhibitors (PMEIs) in the case of pollen tubes [17, 23, 24]). For the sake of simplicity, we assume the cell wall to be incompressible, with a constant cell wall density ρ_w. A minimal description of the viscous cell wall is then embodied in a linear relation between stress resultants and strain rates, which, in the steady state, reads

$$\sigma_{ss} = 4\mu h\left[\frac{du}{ds} + \frac{1}{2}\frac{u\cos\theta}{r}\right],$$

$$\sigma_{\phi\phi} = 4\mu h\left[\frac{1}{2}\frac{du}{ds} + \frac{u\cos\theta}{r}\right], \tag{2}$$

where $u(s)$ is the local tangential velocity of the shell, $h(s)$ is the local cell wall thickness, and $\mu(s)$ is its local viscosity (see Supplemental Data for details). In terms of the defined variables, the strain rates read du/ds and $u\cos\theta/r$.

In order to maintain the growth of the cell, new cell wall material must be supplied to the expanding apical region (Figure 1B). We account for the addition of new cell wall material to the pre-existing wall through an inhomogeneous secretion rate that describes the localized, cytoskeletally guided fusion of secretory vesicles with the plasma membrane [3, 15, 16, 25, 26] (Figure 1B). If $\gamma(s)$ is the local rate of cell wall material addition per unit surface to the pre-existing wall, local mass conservation of the cell wall material dictates that (see Supplemental Data for details)

$$\frac{d(urh)}{ds} = \frac{r\,\gamma}{\rho_w}. \tag{3}$$

Equations 1–3 form a complete set of differential equations for the variables $u(s)$, $r(s)$, and $h(s)$, once the viscosity $\mu(s)$, the material secretion rate $\gamma(s)$, and some boundary conditions are specified.

Wall Secretion Rate: $\gamma(s)$

Despite the complexity of the intracellular phenomena associated with the organization of cytoskeletal filaments, cytoplasmic streaming, and several other processes in the

*Correspondence: lm@seas.harvard.edu

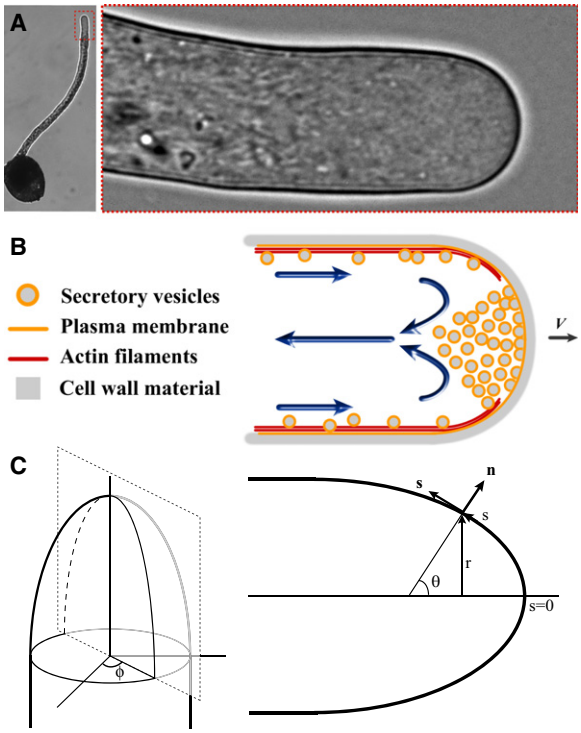

Figure 1. System Geometry and Definitions, Example of Tip-Growing Cell: Pollen Tubes

(A) Lily pollen tube growing from a hydrated pollen grain in vitro and observed with bright-field microscopy (left). The image on the right is a close-up of the apical region and its vicinity (dashed red box). Image courtesy of Enrique Rojas (Dumais Lab, Harvard University).

(B) Sketch of the apical region of a growing pollen tube showing how secretory vesicles (circles) move along actin filaments (red) toward the apex, transporting the cell wall material (gray) and secreting it by fusing to the plasma membrane (yellow) [17, 18]. The motion of secretory vesicles along actin filaments induces a cytoplasmic flow (cytoplasmic streaming; blue arrows) with a characteristic "reverse fountain pattern" that creates an accumulation of secretory vesicles close to the apex.

(C) Parameterization of the cell shape in the apical region. The left panel shows the tridimensional geometry of the growing cell. A section at constant azimuthal angle ϕ (transparent plane) is shown on the right, together with the coordinate system used to describe a point on the surface (in the moving frame located at the apex of the cell), where **n** represents the normal vector to the surface and **s** the tangential direction.

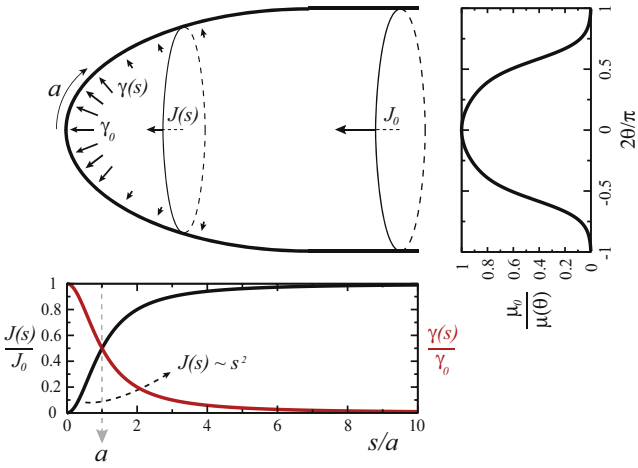

Figure 2. Secretion of Cell Wall Material and Differential Viscosity

Sketch of the apical region of the cell describing the spatial dependence of the two functions that characterize transport and secretion of cell wall material, $J(s)$ and $\gamma(s)$, respectively, and also of the wall viscosity μ. The net total flux of cell wall material going through a cross-section of the cell, $J(s)$, is represented by an arrow in the center of the sketched cross-section, and it is constant (J_0) in the cylindrical region. The secretion of material into the wall is represented by internal arrows in the normal direction. Secretion is maximal at the apex (longer arrows), where the secretion rate per unit surface is constant (γ_0) and decreases considerably at the characteristic length scale a. Examples of the functions $J(s)$ and $\gamma(s)$, with the required asymptotic behaviors and the crossover at the length scale a, are plotted (down). In this example $J(s)/J_0 = s^2/(s^2 + a^2)$. An example of the variation of the viscosity with θ, $\mu(\theta)/\mu_0 = (1 + \theta^6)/\cos\theta$, also with the required asymptotic behavior, is plotted (right; inverse viscosity is plotted for clarity).

neighborhood of the apical region [3, 16, 17, 25, 26], some general properties can be established for the spatial dependence of the secretion rate in a steadily tip-growing cell. In the reference frame attached to tip of the growing cell, the net axial flux of cell wall material through a cross-section of the tube, $J(s)$, is related to the local secretion rate via the expression

$$2\pi r\gamma(s) = \frac{dJ(s)}{ds}, \quad (4)$$

where we have assumed that there is no degradation or synthesis of cell wall material in the cytoplasm, as shown to be valid in the near apical region [3, 18] (see Supplemental Data for details).

Far away from the apex, in the cylindrical part of the cell, there is no material addition ($\gamma = 0$) [3, 17, 18], so that the net flux of cell wall material is a constant J_0 (Equation 4; Figure 2). At the apex, the secretion rate per unit surface is a constant γ_0 because it can neither vanish nor diverge in the steady state. Consequently, following Equation 4, the asymptotic behavior of the flux close to the apex ($s \to 0$ and $\theta \to 0$) is $J(s) \sim s^2$. Between these two limiting cases the spatial profile of the flux (or the secretion rate) may depend on many details [25, 26], but continuity alone implies the existence of a length scale, a, characterizing the crossover from one limiting regime to the other (Figure 2). Over this secretion length scale, a, the secretion rate γ changes significantly compared to its value γ_0 at the apex. This is consistent with the observations in pollen tubes, among other tip-growing cells [3, 19], which show a distinct region in the neighborhood of the apex with a sharp gradient in the density of both secretory and endocytic vesicles [26] (Figure 1B). Although an infinite family of functional forms may be constructed with these minimal constraints, we show below that our qualitative results are unchanged as long as we respect the asymptotic behaviors discussed above.

Wall Viscosity: $\mu(s)$

The mechanical properties of the cell wall at a given position depend on the local concentration of crosslinks between the constituent polymers. In vitro experiments with pectin polymers (the primary constituent of the cell wall in the apical region of pollen tubes [1, 17, 18]) have shown that for crosslink concentrations below a critical value ρ^* the pectin network flows, with a viscosity that depends on the crosslink concentration [27]. At a critical crosslink concentration ρ^* (gelation transition [27, 28]), the pectin network ceases to flow (characterized by a diverging viscosity at the critical point [27]), and when $\rho > \rho^*$ the network behaves as an elastic gel. In pollen tubes, both the concentration of methylesterified pectin

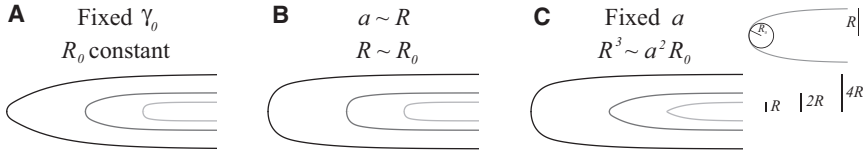

Figure 3. Scaling Laws for Tip Growth

To obtain scaling relations involving only the radius of curvature at the apex, R_0, and the radius of the cell, R, from the general scaling laws (Equation 7), we need to specify the dependence of a on R (or on R_0). We discuss some cases.

(A) If the secretion rate at the apex, γ_0, is a fixed quantity (independent of R or V), which could happen, for instance, by the crowding of secretory vesicles at the apex, then R_0 is constant, independent of R (Equation 5) and $a \sim (R^3/R_0)^{1/2}$, i.e., the larger the radius of the cell, the more pointy it would be.

(B) On the other hand, if the length a scales with the cell radius ($a \sim R$), as can be envisioned by considering that the intracellular processes that determine a vary with the radius of the cell, then $R \sim R_0$, i.e., cells would have the same shape independent of their size.

(C) If a was constant, independent of the cell radius, then $R^3 \sim a^2 R_0$, i.e., the larger the cell, the flatter its apex would be.

(noncrosslinked pectin) and the concentration of PMEIs decrease monotonically from the apex [23, 24]. Assuming the extracellular calcium concentration to be homogeneous, the concentration of crosslinks in the cell wall of pollen tubes increases monotonically from the apex, and so does then the wall viscosity. Therefore, far away from the expanding apical region, the cell wall of pollen tubes does not flow anymore and adopts a cylindrical, tubular shape compatible with a pressurized elastic cylinder. We interpret the transition from a fluid-like to a solid-like behavior as occurring when the crosslink concentration exceeds the critical crosslink concentration ρ^* at the gelation transition, consistent with experimental observations [27]. The effect of PMEIs in pollen tubes, and most likely of other cell wall loosening enzymes in different organisms, is therefore not to soften the cell wall, but to *fluidize* it, which involves a sol-gel-like phase transition rather than just a mere change of material stiffness.

Close to the apex, the fluid cell wall is characterized by a finite viscosity μ_0. In agreement with the fact that the cell wall behaves as a pressurized elastic shell far away from the growing apical region, the dynamics of cell wall expansion described by Equations 1, 2, and 3 require the viscosity to diverge (gelation of the cell wall) as the cell shape approaches the characteristic tubular geometry away from the apex. Mathematically, this translates into a viscosity μ that diverges as $\mu(\theta) \sim 1/(\pi/2 - \theta)$ when approaching the tubular geometry ($\theta \rightarrow \pi/2$ and $\kappa_s \rightarrow 0$). For the sake of simplicity, we assume that the tubular geometry is attained asymptotically far away from the apex ($s \rightarrow \infty$). We note that the dependence of μ on space is implicit through other fields, such as the concentration of the enzymes that control the local crosslinking state of the cell wall, and therefore its functional form may depend on s, θ, and/or r, or a combination of them. Assuming that the kinetics of crosslinking in the cell wall are much faster than all other time scales in the problem allows us to write $\mu = \mu(\theta)$ without explicitly introducing any additional parameters.

Scales and Scaling Laws

Tip Geometry

Close to the apex of the cell, the local geometry is that of a sphere with radius of curvature R_0 and curvature $\kappa_0 = 1/R_0$. The steady apical expansion of a cell wall with density ρ_w and viscosity μ_0 driven by the turgor pressure P is maintained by a constant supply of cell wall material per unit surface γ_0. Comparing the velocity at which cell wall material is assembled, γ_0/ρ_w, to the expansion rate of the wall, P/μ_0, yields a length scale $R_0 \sim \mu_0\gamma_0/P\rho_w$, the tip radius of curvature. Indeed, using Equations 1, 2, and 3, we may verify this because the asymptotic solutions close to the apex are $\theta(r) = \kappa_0 r$, $u(r) = u'_0 r$ and $h(r) = h_0$, with

$$\kappa_0 = \frac{P\rho_w}{6\mu_0\gamma_0} \quad \text{and} \quad u'_0 = \frac{\gamma_0}{2h_0\rho_w}, \tag{5}$$

where u'_0 characterizes the spatial velocity gradient of tangential cell wall expansion near the tip and h_0 is the cell wall thickness at the apex. The curvature κ_0 and u'_0 set the velocity scale u_0 in the shell, which reads $u_0 = u'_0/\kappa_0 = 3\mu_0\gamma_0^2/P\rho_w^2 h_0$. We note that the absolute scale of cell wall thickness, h_0, cannot be fixed in our framework because we do not discuss the microscopic mechanism of cell wall formation and turnover in the through-the-thickness direction. However, the spatial variations in cell wall thickness are accounted for in our theory through mass conservation.

Tubular Geometry

Far away from the apical region, the cell wall does not flow and becomes a cylindrical, tubular, elastic shell with radius R and thickness H. In the reference frame attached to the apex, the velocity V of the tubular region corresponds to the growth velocity of the cell. Comparing the wall expansion rate, P/μ_0, to the total available cell wall volume per unit time, J_0/ρ_w, sets a tubal length scale $(J_0\mu_0/\rho_w P)^{1/3}$. Indeed, rewriting Equations 1, 2, and 3 for a cylindrical shape and taking into account the asymptotic behavior of the viscosity in this region yields

$$R^3 = \frac{2}{\pi}\frac{\mu_0 J_0}{P\rho_w}. \tag{6}$$

Although the quantities P, μ_0, and ρ_w are intrinsic constants and do not depend on the geometry, size, or velocity of the cell, the total net flux J_0 (and similarly γ_0) does, in general, depend on them. Therefore, in order to separately specify the radius R and velocity V of the cell only in terms of intrinsic quantities, it is necessary to establish the dependence of J_0 on R and V, which we discuss below.

Scaling Laws

Using Equations 5 and 6, and relating γ_0 to J_0 through $\pi a^2\gamma_0 = J_0$ (Equation 4), we obtain the scaling laws

$$\frac{R}{R_0} \sim \left(\frac{a}{R_0}\right)^{2/3} \quad \text{and} \quad \frac{V}{u_0}\frac{H}{h_0} \sim \left(\frac{a}{R_0}\right)^{4/3}. \tag{7}$$

These hold for any form of the flux $J_0(R, V)$ and measure the pointedness of the cell and the cell wall material flow rate, respectively, as a function of the ratio a/R_0, which compares the secretion length scale a to the wall expansion length scale R_0. Because they follow from simple considerations of mass and force balance in the apical and tubular regions, they are broadly applicable. In Figure 3 we discuss some cases of particular interest.

Cell Radius and Velocity

As an example of the relation between flux and cell growth velocity and size, we consider the case of *cortical transport* characteristic of pollen tubes [1, 17, 18, 29], in which secretory vesicles are transported toward the apex along the actin filaments forming a shell underneath the plasma membrane (Figure 1B). In such a case, the net flux of material transported toward the apex reads $J_0 = 2\pi R \rho_0 (V_0 - V)$, where ρ_0 is the surface density of cell wall material being transported (proportional to the surface density of secretory vesicles) and V_0 is the velocity of the secretory vesicles, which is mainly determined by the velocity of the myosin motors carrying them [17]. For the case of *cortical transport*, the radius and velocity of the tip-growing cell are related by

$$R^2 = 4\frac{\mu_0 V_0}{P}\frac{\rho_0}{\rho_w}\left(1 - \frac{V}{V_0}\right), \qquad (8)$$

which follows from Equation 6. If the typical growth velocity V of the cell is much smaller than V_0 ($V \ll V_0$), as commonly observed experimentally for pollen tubes, we see that the radius of the cell becomes essentially independent of its growth velocity. Explicit expressions for the radius and velocity can be obtained by combining Equations 1, 2, and 3 and the function $J_0(R, V)$.

Cell Shape

To go beyond our scaling analysis and determine the shapes of the growing apical region, it is necessary to specify the functions $\mu(s)$ and $\gamma(s)$ (or $J(s)$ equivalently). We use the functional forms $J(s) = J_0 s^2/(s^2 + a^2)$ and $\mu(\theta) = \mu_0(1 + \theta^6)/\cos\theta$ for the numerical calculations (Figure 2). Although the particular cell shape will depend on the choice of these functions, we find that the same qualitative results are obtained for any reasonable functional forms consistent with the asymptotic behaviors described above for the wall secretion rate and viscosity (see Supplemental Data).

The ratio of the length scale, a, that characterizes the spatial variation of secretion of new cell wall material and the characteristic radius of curvature R_0, which arises from the mechanics of cell wall expansion, defines the dimensionless parameter $\alpha \equiv a/R_0$. Once we have scaled the curvatures with the tip curvature κ_0, h with the microscopically determined wall thickness h_0, and u with the cell wall expansion velocity at the tip u_0, α is the only dimensionless parameter left in the problem. Figure 4A shows the dependence of the numerical solutions of Equations 1, 2, and 3 on α. For $\alpha \lesssim 1$ the shapes show a characteristically flatter region in the vicinity of the apex, which translates into a nonmonotonic curvature κ_s. This is consistent with observations in pollen tubes and root hairs [30] (see Supplemental Data) and may be interpreted in terms of the competition between local cell wall assembly and expansion. The nonmonotonicity of the curvature leads to nonmonotonous strain rates (see Supplemental Data) and cell wall thickness (Figure 4), even though the viscosity increases monotonically away from the apex (Figure 4) and the material secretion rate decreases monotonically (Figure 2). As α is increased, the shapes become increasingly pointed, with a monotonically decreasing curvature κ_s from its maximal value κ_0 at the apex (Figure 4A). In this case, the velocity profile shows two distinct regimes, with a fast linear increase at the apex and a slow convergence to its maximal velocity V. Both flat and pointed apices are observed in the tip growth of different organisms [19, 20, 30],

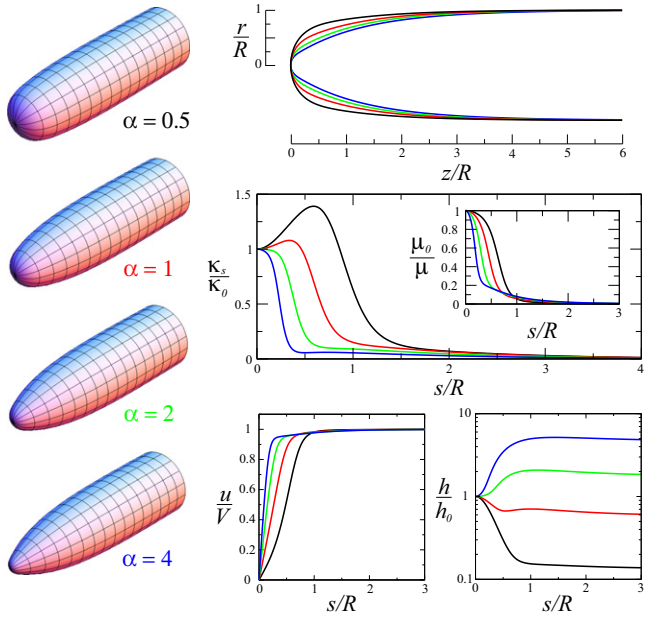

Figure 4. Numerical Solutions

Apical cell shapes obtained numerically for different values of the parameter $\alpha \equiv a/R_0$ (top right): $\alpha = 0.5$ (black), $\alpha = 1$ (red), $\alpha = 2$ (green), and $\alpha = 4$ (blue). The shapes are also shown in 3D for clarity (left). Small values of α correspond to flatter apices, whereas large values of α are associated with pointy cells. The curvature $\kappa_s(s)$, the tangential expansion velocity of the cell wall, $u(s)$, and the cell wall thickness, $h(s)$, are shown for the different shapes. The viscosity $\mu(s)$ is plotted as a function of the arclength (inset in the plot showing κ_s; inverse viscosity is plotted for clarity), showing a monotonic increase from the apex even when the curvature is nonmonotonic. The functions $J(s)$ and $\mu(\theta)$ used to obtain the numerical solutions are those in Figure 2 and explained in the main text.

suggesting that our minimal theoretical considerations are sufficient to explain these morphologies.

Discussion

A molecular approach to cellular morphogenesis requires knowledge of the dynamics of cytoskeletal structures and their control via signaling molecules that would allow us to build up toward a description of cell shape and its evolution. Unfortunately, many of the putative intracellular processes that control wall material production, transport, and assembly are not yet well understood. However, it may be argued that even if they were understood, it is extremely improbable that all this detailed information is required to address global questions such as the cell size, shape, and dynamics, which require global constraints ([3]; Figure 5). Mesoscopic approaches, while ignoring some of the molecular details, provide a possible route that allows us to identify the biophysical parameters that control the scales and the diversity of shapes in tip growth.

Our description of tip growth avoids the molecular approach in favor of a mesoscopic view by assuming that the effect of intracellular processes can be described effectively by two functions, which account for the local secretion rate and the rheology of the cell wall (Figure 5). The shape of the cell may depend on many details through the functional forms of the viscosity μ and the secretion rate γ. However, the scaling laws (Equation 7), the dependence of the cell radius and velocity on the physical parameters (Equation 8), and the variation of

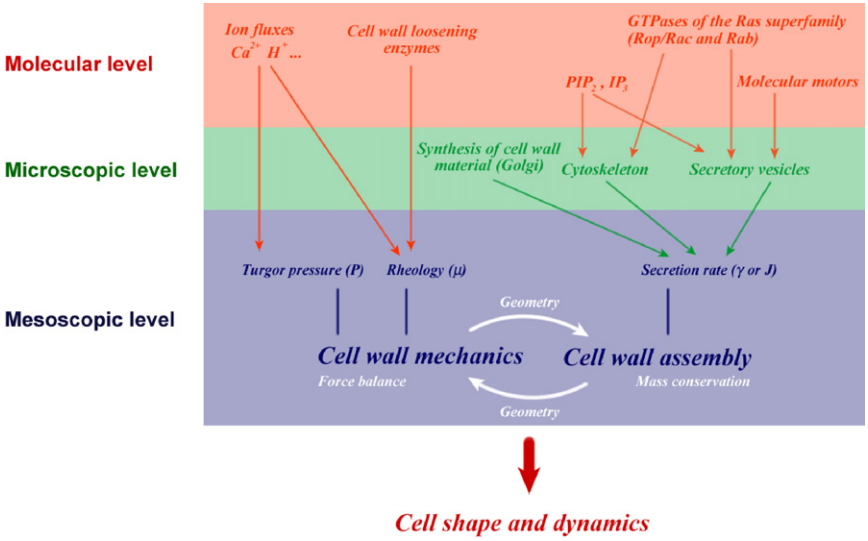

Figure 5. Schematic Representation of the Different Description Levels of Tip Growth

This sketch only contains the most straightforward relations between the molecules and processes that control cell morphogenesis. There are some relations (arrows in the sketch) between these elements that have been omitted for the sake of simplicity or because they are not yet established. Similarly, it is possible that other processes that are likely to play a role in shaping the cell have not been considered in the sketch, either because they are not known or because their role is thought to be minor compared to those sketched here. As important as the extensively studied molecular and microscopic levels, at the mesoscopic scale the assembly and extension of the cell wall are governed by the laws of physics. No matter how complex intracellular processes and signaling pathways may be, the morphogenesis of the cell must obey essential incontrovertible laws at the mesoscopic scale, such as force balance and mass conservation. Whereas these generic laws set the possible shapes for the cell, molecular cues establish the actual shape of the cell from the possible, physically meaningful shapes. The molecular control of cellular morphogenesis occurs through the modification of the effective mesoscopic parameters, namely, the turgor pressure P, the cell wall rheology (characterized by the local wall viscosity μ), and the local secretion rate γ. Turgor pressure is essentially regulated by ion fluxes (Ca^{2+}, H^+, etc.), which change the osmotic balance between the cell interior and its external environment [3, 17, 18]. The local rheological properties of the cell wall depend on (extracellular) ionic concentrations, and the activity of enzymes that affect the local crosslink concentration in the cell wall (e.g., PMEs and their associated inhibitors in pollen tubes [23, 24]). The cell wall secretion rate is mainly affected by polysaccharide synthesis, the transport of secretory vesicles toward the apex, and the fusion of vesicles with the plasma membrane. Intracellular transport relies on cytoskeletal filaments (regulated at the molecular scale by PIP_2 and IP_3, as well as by small GTPases of the Ras superfamily [17, 31]) and molecular motors (whose activity is known to depend on Ca^{2+} concentration), which carry secretory vesicles to the apical region. Vesicle fusion at the plasma membrane is required for cell wall secretion and is thought to be controlled by GTPases (Rab) and (intracellular) ionic concentrations [17, 31].

the shape with the parameter a/R_0 (Figure 4) are independent of those details, providing robust predictions that can be tested experimentally. Furthermore, the obtained apical geometry (Equation 5) establishes the dependence of two commonly measured quantities [30]—namely, the radius of curvature at the apex, R_0, and the slope of the cell wall expansion velocity $u(s)$, u'_0—on measurable physical parameters, such as turgor pressure P or the secretion rate per unit surface γ_0. These behaviors for both the shape and the expansion velocity in the vicinity of the apex have indeed been observed experimentally [30] (see Supplemental Data). Finally, we show that a single dimensionless parameter, which characterizes the interplay of cell wall mechanics and assembly, may be sufficient to explain much of the diversity of shapes in tip-growing cells.

Our theory sharpens the quest for the molecular underpinnings of morphogenesis by identifying the physical mechanisms in shaping the cell and thus focusing further attention on those molecular pathways involved in the control of the relevant physical magnitudes, such as the local secretion rate and cell wall rheology. Moreover, it provides a framework that can be generalized to other questions of the morphogenesis of walled cells such as diffuse growth, budding, and branching.

Supplemental Data

Supplemental Data include supplemental theory and nine figures and can be found with this article online at http://www.cell.com/current-biology/supplemental/S0960-9822(09)01983-6.

Acknowledgments

We thank Jacques Dumais and Enrique Rojas for discussions and for the images of pollen tubes in Figure 1, as well as the Human Frontiers Science Program and the Harvard NSF-MRSEC for partial financial support.

Received: March 31, 2009
Revised: October 14, 2009
Accepted: October 20, 2009
Published online: December 17, 2009

References

1. Taiz, L., and Zeiger, E. (2006). Plant Physiology, Fourth Edition (Sunderland, MA: Sinauer Associates, Inc).
2. Alberts, B., Bray, D., Lewis, J., Raff, M., Roberts, K., and Watson, J.D. (2004). Molecular Biology of the Cell, Third Edition (New York: Garland).
3. Harold, F.M. (2005). Molecules into cells: Specifying spatial architecture. Microbiol. Mol. Biol. Rev. *69*, 544–564.
4. Fowler, J.E., and Quatrano, R.S. (1997). Plant cell morphogenesis: Plasma membrane interactions with the cytoskeleton and cell wall. Annu. Rev. Cell Dev. Biol. *13*, 697–743.
5. Baskin, T.I. (2005). Anisotropic expansion of the plant cell wall. Annu. Rev. Cell Dev. Biol. *21*, 203–222.
6. Cosgrove, D.J. (2005). Growth of the plant cell wall. Nat. Rev. Mol. Cell Biol. *6*, 850–861.
7. Mathur, J. (2004). Cell shape development in plants. Trends Plant Sci. *9*, 583–590.
8. Thompson, D.W. (2002). On Growth and Form (New York: Dover Publications), reprint of 1942 2nd ed. (1st ed., 1917).
9. Bernal, R., Rojas, E.R., and Dumais, J. (2007). The mechanics of tip growth morphogenesis: What we have learned from rubber balloons. Journal of Mechanics of Materials and Structures *2*, 1157–1168.
10. Goriely, A., and Tabor, M. (2003). Self-similar tip growth in filamentary organisms. Phys. Rev. Lett. *90*, 108101.
11. Lockhart, J.A. (1965). An analysis of irreversible plant cell elongation. J. Theor. Biol. *8*, 264–275.
12. Tindemans, S.H., Kern, N., and Mulder, B.M. (2006). The diffusive vesicle supply center model for tip growth in fungal hyphae. J. Theor. Biol. *238*, 937–948.
13. Gierz, G., and Bartnicki-Garcia, S. (2001). A three-dimensional model of fungal morphogenesis based on the vesicle supply center concept. J. Theor. Biol. *208*, 151–164.
14. Pelce, P., and Pocheau, A. (1992). Geometrical approach to the morphogenesis of unicellular algae. J. Theor. Biol. *156*, 197–214.

15. Mathur, J., and Hülskamp, M. (2002). Microtubules and microfilaments in cell morphogenesis in higher plants. Curr. Biol. *12*, R669–R676.
16. Cole, R.A., and Fowler, J.E. (2006). Polarized growth: Maintaining focus on the tip. Curr. Opin. Plant Biol. *9*, 579–588.
17. Krichevsky, A., Kozlovsky, S.V., Tian, G.W., Chen, M.H., Zaltsman, A., and Citovsky, V. (2007). How pollen tubes grow. Dev. Biol. *303*, 405–420.
18. Hepler, P.K., Vidali, L., and Cheung, A.Y. (2001). Polarized cell growth in higher plants. Annu. Rev. Cell Dev. Biol. *17*, 159–187.
19. Trinci, A., and Saunders, P. (1977). Tip growth of fungal hyphae. J. Gen. Microbiol. *103*, 243–248.
20. Heath, I.B., and Geitmann, A. (2000). Cell biology of plant and fungal tip growth—getting to the point. Plant Cell *12*, 1513–1517.
21. Cabeen, M.T., and Jacobs-Wagner, C. (2005). Bacterial cell shape. Nat. Rev. Microbiol. *3*, 601–610.
22. Cosgrove, D.J. (2000). Loosening of plant cell walls by expansins. Nature *407*, 321–326.
23. Bosch, M., and Hepler, P.K. (2005). Pectin methylesterases and pectin dynamics in pollen tubes. Plant Cell *17*, 3219–3226.
24. Röckel, N., Wolf, S., Kost, B., Rausch, T., and Greiner, S. (2008). Elaborate spatial patterning of cell-wall PME and PMEI at the pollen tube tip involves PMEI endocytosis, and reflects the distribution of esterified and de-esterified pectins. Plant J. *53*, 133–143.
25. Campanoni, P., and Blatt, M.R. (2007). Membrane trafficking and polar growth in root hairs and pollen tubes. J. Exp. Bot. *58*, 65–74.
26. Bove, J., Vaillancourt, B., Kroeger, J., Hepler, P.K., Wiseman, P.W., and Geitmann, A. (2008). Magnitude and direction of vesicle dynamics in growing pollen tubes using spatiotemporal image correlation spectroscopy and fluorescence recovery after photobleaching. Plant Physiol. *147*, 1646–1658.
27. Axelos, M.A., and Kolb, M. (1990). Crosslinked biopolymers: Experimental evidence for scalar percolation theory. Phys. Rev. Lett. *64*, 1457–1460.
28. de Gennes, P.G. (1979). Scaling Concepts in Polymer Physics (Ithaca, NY: Cornell University Press).
29. Vidali, L., McKenna, S.T., and Hepler, P.K. (2001). Actin polymerization is essential for pollen tube growth. Mol. Biol. Cell *12*, 2534–2545.
30. Dumais, J., Long, S.R., and Shaw, S.L. (2004). The mechanics of surface expansion anisotropy in Medicago truncatula root hairs. Plant Physiol. *136*, 3266–3275.
31. Lee, Y.J., and Yang, Z. (2008). Tip growth: Signaling in the apical dome. Curr. Opin. Plant Biol. *11*, 662–671.

Current Biology, Volume *19*
Supplemental Data

Shape and Dynamics of Tip-Growing Cells

O. Campàs and L. Mahadevan

1 Derivation of force and mass balance laws

Here we provide a self-contained derivation of the basic balance equations in the main text.

1.1 Local force balance (Eq. 1 of the main text)

Experimental observations show that the typical thickness of the cell wall ($0.1-1\,\mu$m) is much smaller that the typical radius of curvature of tip growing cells, which is of the order of $10\,\mu$m. The cell wall can thus be described as a thin shell from the geometrical viewpoint. Along the cell wall, viscous forces dominate over inertial effects at the small micrometric length scales and slow velocity (micrometers/s) scales involved in cell growth. Thus forces must always sum up to zero during the process of cell growth.

At each point of the cell wall the turgor pressure P leads to a normal stress in the outward direction (Fig. S1 A,C) and also generates tensions σ_{ss} and $\sigma_{\phi\phi}$ along the two principal directions of the surface, the tangential direction, $\mathbf{s}$, and the azimuthal direction, ϕ (in the third principal direction, normal to the shell, the stress is simply the pressure itself). To write down the consequence of force balance locally along the principal directions, we first note that the infinitesimal area element $da = rd\phi ds$ where ds is the size of the infinitesimal element in the tangential direction and $rd\phi$ is the size of the infinitesimal element in the azimuthal direction (Fig. S1 A,B). Let $d\theta$ be the differential angle defined between the tangents (in the $\mathbf{s}$ direction) to the surface at the locations s and $s+ds$ (Fig. S1 B). Then

$$d\theta = \frac{d\theta}{ds}\, ds = \kappa_s\, ds\,, \tag{S1}$$

where $\kappa_s = d\theta/ds$ is the local curvature along s [1]. The projected force in the normal direction due to the tension σ_{ss} is given by $\sigma_{ss} d\theta\; rd\phi = \sigma_{ss}\kappa_s rd\phi ds$ (Fig. S1 B,C). Similarly, when we consider the azimuthal direction, with an azimuthal curvature κ_ϕ, the projected force in the normal direction due to the azimuthal stress is $\sigma_{\phi\phi}\kappa_\phi rd\phi ds$. Balancing the cumulative contributions of the

tensions in both principal directions, $\mathbf{s}$ and ϕ, with the contribution from turgor $P\,da = P\,r d\phi ds$ yields

$$P = \kappa_s \sigma_{ss} + \kappa_\phi \sigma_{\phi\phi}\,, \tag{S2}$$

which corresponds to the first equation in Eq. 1 of the main text.

The second equation in Eq. 1 of the main text corresponds to force balance in the direction of growth. If we consider a section of the tip growing cell at a certain distance from the apex (Fig. S1 D), the cumulative contribution to the force in the growth direction due to the turgor pressure over the apical cup defined by such a section is given by

$$\int dS\, P\, \cos\theta = 2\pi P \int_0^{r(s)} ds\, r \cos\theta = 2\pi P \int_0^{r(s)} dr\, r = P\pi r^2\,, \tag{S3}$$

where we used the relation $dr/ds = \cos\theta$. This cumulative force must be balanced by the projection of the tension in the $\mathbf{s}$ direction, σ_{ss}, at the boundary defined by the section (Fig. S1 D; [2, 3]), which reads

$$2\pi r \sigma_{ss} \sin\theta\,. \tag{S4}$$

Balancing the contributions S3 and S4, one obtains

$$\frac{P}{2} = \kappa_\phi \sigma_{ss}\,, \tag{S5}$$

where we used the expression $\kappa_\phi = \sin\theta/r$.

We note that the theory described in the main text and detailed above ignores the effects of any bending resistance that the shell might have. Indeed, the bending contribution is relevant in regions where the characteristic length of shell deformation, R, is smaller or about $\sqrt{Rh}$ [2]. As the typically observed radii of curvature for pollen tubes are about $10\,\mu$m, leading to $\sqrt{Rh} \sim 1\,\mu$m, bending contributions can be neglected.

1.2 Stress-strain rate relations (Eq. 2 of the main text)

At a minimal level, we describe the cell wall as a simple viscous fluid with a viscosity that changes with location following the distribution of cell wall loosening enzymes. In the case of a fluid shell, the strain rates (elemental rates of deformation) ϵ_s and ϵ_ϕ, along the two principal directions, $\mathbf{s}$ and ϕ, are given by

$$\epsilon_s = \frac{du}{ds} \quad \text{and} \quad \epsilon_\phi = \frac{u\cos\theta}{r}\,, \tag{S6}$$

at steady state. The strain rate ϵ_s expresses how much the cell wall is stretched per unit time along the tangential direction s; indeed, it is the difference in velocity between two adjacent points, i.e., du/ds, that quantifies how much the stretch between two adjacent points changes per unit time along the tangential direction s. Similarly, the strain rate ϵ_ϕ expresses how much the cell wall is stretched per unit time in the radial direction r: the rate of expansion of the

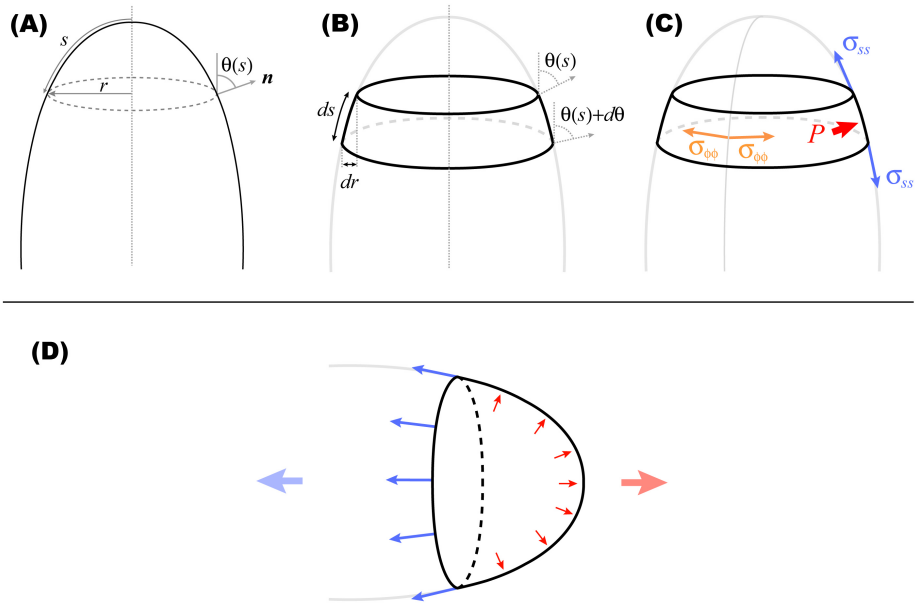

Figure S1: **Local force balance.** (A) Sketch of the apical region of a tip growing cell, where the contour length s, the cell thickness r and the angle θ between the local normal $\mathbf{n}$ and the direction of growth are indicated. (B) Definition of the infinitesimal elements ds, dr and $d\theta$, associated to infinitesimal changes of the variables s, r and θ respectively. (C) Sketch of the forces acting on an element of the surface. The turgor pressure P (red arrow) is along the outward normal direction to the surface. The tension σ_{ss} (blue arrows) acts along the tangential direction ($\mathbf{s}$) at every point, and the tension $\sigma_{\phi\phi}$ (orange arrows) acts along the azimuthal direction (ϕ) at every point. The existence of local curvatures κ_s and κ_ϕ allows the local tensions σ_{ss} and $\sigma_{\phi\phi}$ to contribute along the normal direction and balance the turgor pressure, as explained in the text. (D) Force balance along the direction of cell growth. Forces generated by turgor pressure are along the local normal direction of the surface (small red arrows); their cumulative contribution along the direction of cell growth is depicted with a big light red arrow. The cell wall tension σ_{ss} along the tangential direction, at the boundary of the defined cross-section, is represented by long blue arrows. The cumulative contribution of this tension over the cross-section, projected along the direction of cell growth, is depicted as a light blue arrow. The cumulative contribution in the direction of growth of the turgor pressure over the apical cup defined by the cross-section (light red arrow), is balanced by the projection of the cumulative contribution of the cell wall tension σ_{ss} (light blue arrow), as explained in the text.

cell wall in the radial direction at a given point is simply given by the projection of the expansion velocity u in the radial direction r, which reads $u\cos\theta$, so that the relative expansion of the cell wall in the radial direction is given by $\epsilon_\phi = u\cos\theta/r$.

To complete the formulation of the equations of motion, we then need to relate the tensions in the shell to the elemental rates of deformation (the strain rates). The simplest relations, which follow from our assumption of linear stress-strain rate relations for a viscous (Newtonian) fluid [4], are

$$\sigma_{ss} = 4\mu h\left[\epsilon_s + \frac{1}{2}\,\epsilon_\phi\right] \quad \text{and} \quad \sigma_{\phi\phi} = 4\mu h\left[\frac{1}{2}\,\epsilon_s + \epsilon_\phi\right], \tag{S7}$$

where μ is the local viscosity of the cell wall and the tensions σ_{ss} and $\sigma_{\phi\phi}$ are obtained by integration across the through-the-thickness direction of the stresses in the respective principal directions. The integration of the stresses to obtain the tensions explains the contributions of each strain rate to the tension in a given principal direction. In particular, the strain rate in the same principal direction that the tension contributes with a factor $4h$ (the factor 4 is known as the Trouton ratio and relates the extensional viscosity to the shear viscosity), while the remaining strain rate contributes with $2h$ in the case of an incompressible fluid [5].

1.3 Mass conservation (Eq. 3 of the main text)

In order to derive Eq. 3 of the main text, consider a slice of the growing cell of differential thickness ds, as sketched in Fig. S2 A. In the steady state, the difference of fluxes $j_s(s+ds) - j_s(s)$ flowing across the circular slice of cell wall in the s direction must equal the flux of mass being added to the same slice of cell wall per unit time, which reads $2\pi r(s)\gamma(s)ds$ (with $\gamma(s)$ being the amount of new cell wall material added to the preexisting wall per unit surface and unit time), so that

$$j_s(s+ds) - j_s(s) = 2\pi r(s)\gamma(s)ds\,, \tag{S8}$$

which in the limit $ds \to 0$ yields the steady state relation:

$$\frac{dj_s(s)}{ds} = 2\pi r(s)\gamma(s)\,. \tag{S9}$$

The convective flux of cell wall material flowing along the tangential direction, $\mathbf{s}$, across the considered circular slice is given by

$$j_s(s) = 2\pi r(s)h(s)\,\rho_w\,u(s)\,, \tag{S10}$$

where ρ_w is the cell wall density, assumed to be constant for the sake of simplicity. Combining Eqs. S9 and S10, we obtain Eq. 3 of the main text, i.e.,

$$\frac{d\,(rhu)}{ds} = \frac{r\gamma}{\rho_w}\,. \tag{S11}$$

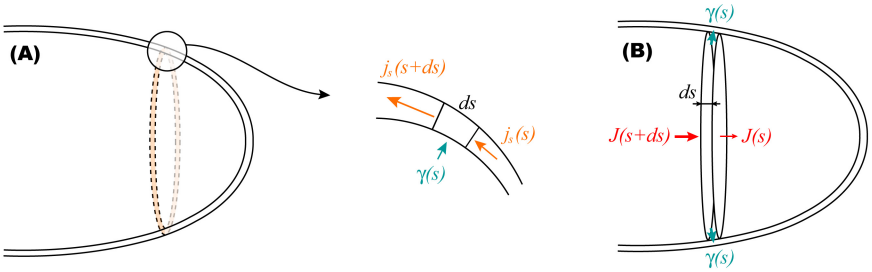

Figure S2: **Local mass conservation.** (A) Sketch of the apical region of a tip growing cell. The magnified region represents a close up of the cell wall where we depict the fluxes of cell wall material getting in and out of a cell wall element with differential length ds. In particular, the fluxes of cell wall material that this differential cell wall element exchanges with the neighboring cell wall are $j_s(s)$ and $j_s(s+ds)$, while the cell wall material exchange with the cytoplasm is given by $\gamma(s)$. In the steady state, the balance of fluxes requires that the difference between outgoing and incoming cell wall fluxes in any differential cell wall element, i.e., $j_s(s+ds) - j_s(s)$, must be accounted for by the secretion flux $\gamma(s)\, ds$. (B) Given two cross-sections of the cell, separated by a differential distance ds, any difference between the net cytoplasmic flow of cell wall material along the direction of growth across the defined cross-sections, i.e., $J(s) - J(s+ds)$, must be due to secretion to the preexisting cell wall.

1.3.1 Relation between $J(s)$ and $\gamma(s)$ (Eq. 4 of the main text)

Here we explain the relation between the net axial flux of cell wall material through a cross-section of the cell (in the reference frame attached to tip of the growing cell), $J(s)$, and the secretion rate per unit surface $\gamma(s)$. Consider two adjacent cross-sections of the cell separated by a differential length ds along the cell contour (Fig. S2 B). The difference between the net cytoplasmic flux of cell wall material crossing the two sections is $J(s+ds) - J(s)$. Conservation of the cell wall material in the cytoplasm of the apical region imposes that any difference between the flux $J(s+ds)$ and $J(s)$ must have left the cytoplasm through the boundary that connects the two adjacent sections, i.e., it must have been secreted to the preexisting wall. As the secretion flux in the annular region between the two defined cross-sections is given by $2\pi r\gamma(s)\, ds$, we obtain

$$\frac{dJ\,(s)}{ds} = 2\pi r\gamma(s)\,, \tag{S12}$$

by equating the difference $J(s+ds) - J(s)$ to the flux being secreted to the pre-existing wall and taking the limit $ds \to 0$. This relation assumes no production or degradation of cell wall material in the cytoplasm of the apical region. This assumption is supported by experimental observations showing that the new cell wall material is produced far away from the growing region and transported actively to the growing apex along cytoskeletal filaments.

2 Comparison of numerical solutions to the experimental data for root hairs

Pollen tubes are not the only example of tip growth in plants; root hairs, also elongate using the same strategy. Experiments with root hairs have shown that the meridional curvature is non-monotonic (Figure 3). This has led to suggestions that one needs a non- monotonic rheology to explain this behavior. Here we show that the experimental observations on the tip growth of root hairs [6, 7] are in agreement with our theoretical results, and do not require any such assumptions; the observed behavior follows from simple monotonic variations in the viscosity and secretion rates as one moves away from the tip.

Fig. S3 compares the experimental measurements of the meridional curvature (κ_s), the meridional velocity (cell wall expansion velocity $u(s)$) and the strain rates (ϵ_s and ϵ_ϕ) as a function of the arc length position (s) in root hairs [6], to the results obtained by numerical integration of Eqs. 1, 2 and 3 (of the main text) for $\alpha = 0.8$ (the functional forms of μ and J are the same as in Fig. 4 of the main text). All measured quantities agree qualitatively, and even semi-quantitatively, with the theoretical results. In particular, we show that the predicted strain rates (or elemental rates of expansion) ϵ_s and ϵ_ϕ show a non-monotonous behavior, with maximal strain rates located in an annulus surrounding the polar axis, even for a secretion rate $\gamma(s)$ that decreases monotonically from the apex and a viscosity $\mu(s)$ that increases monotonically from the apex. Indeed, the wall viscosity is likely to increase monotonically as it follows the crosslink concentration in the wall, which is observed to increase monotonically.

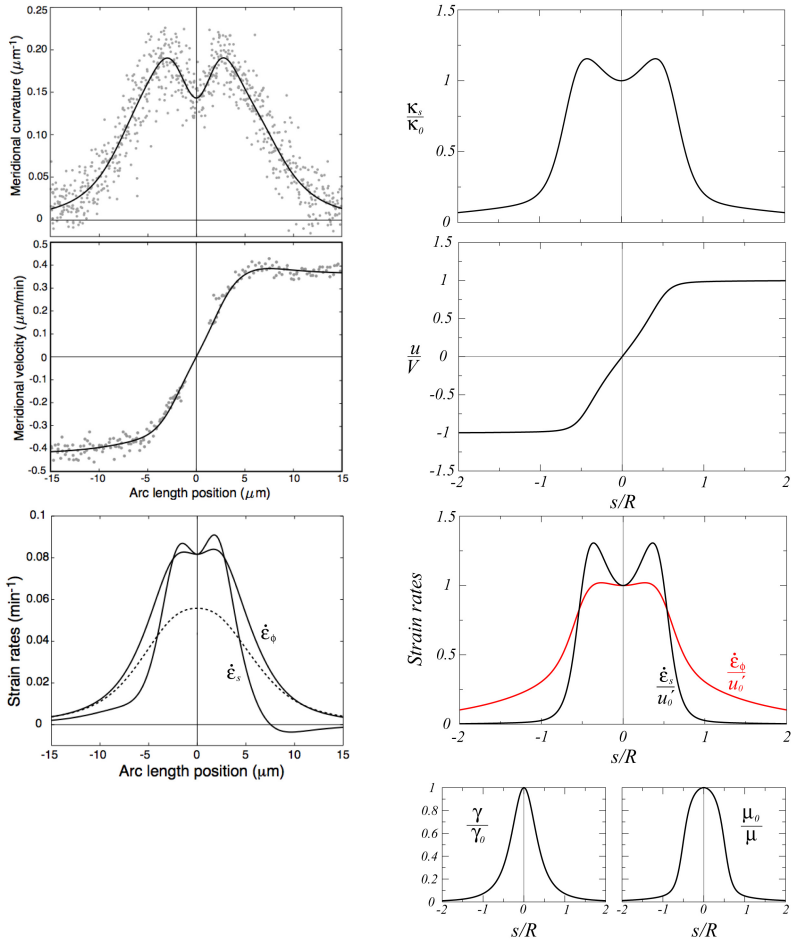

Figure S3: **Comparison of the experimental results on the tip growth of root hairs [6, 7] to our theoretical results.** The panels on the left show the experimental measure of the meridional curvature (κ_s), the meridional velocity (cell wall expansion velocity $u(s)$) and the strain rates (ϵ_s and ϵ_ϕ) as a function of the arc length position (s) (First reproduced at Journal of Mechanics of Materials and Structures vol. 2 page 1157. Reproduced here with permission). The panels on the right show the numerical solution for each of the magnitudes shown on the left panels. The numerical solutions were obtained by numerical integration of Eqs. 1, 2 and 3 (of the main text) for $\alpha = 0.8$, using the same functional forms of μ and J as in Fig. 4 of the main text.

3 Variation of pollen tube shape with α, for different functional forms of the viscosity $\mu(s)$ and the flux of cell wall material $J(s)$

The detailed shape of a pollen tube in the apical region depends on both the spatial and temporal distribution of cell wall material secretion rate $\gamma(s,t)$ and the variation of the cell wall rheology (in our minimal description, the viscosity $\mu(s,t)$) with location and time. In the main text we showed that the variation of the pollen tube shapes may be characterized in terms of just one dimensionless parameter in the problem, $\alpha \equiv a/R_0$. We show here that although the particular shape of the apical region depends on the spatial dependence of both the secretion rate of cell wall material (or equivalently, the flux $J(s)$) and the wall viscosity μ, the variation of the pollen tube shape with the parameter α is independent of the particular choice of these functional forms.

To this end, we solve the steady-state equations derived in the main text (Eq. 6) for different representative choices of the functions $J(s)$ and $\mu(\theta)$ (Fig. S4). All of the chosen functions have the following asymptotic behaviors: (i) close to the apex or tip ($s \to 0$) the flux J scales like $J(s) \sim s^2$ (this condition is equivalent to $\gamma(s) \to \gamma_0$ as $s \to 0$) and the viscosity approaches a constant value μ_0 ($\mu(s) \to \mu_0$ as $s \to 0$); (ii) far away from the apex, in the tubular region ($s \to \infty$) the flux of cell wall material going through a cross-section of the tube is constant and given by J_0, so that $J(s \to \infty) \to J_0$, and the viscosity must diverge as $\mu(s) \sim 1/\left(\pi/2 - \theta(s)\right)$ for $s \to \infty$. This divergence of the viscosity simply reflects the fact that the cell wall becomes rigid in the tubular region far away from the apex.

The set of functions chosen cover the extreme range of features. For the flux $J(s)$ (Fig. S4 A), while the asymptotic behavior close to the apex is fixed, the way the flux saturates to J_0 is not restricted. We specify two functions with qualitatively different behaviors as far as saturation is concerned: a slow, power-law saturation $J(s) = J_0\, s^2/(s^2 + a^2)$ and a fast, exponential saturation $J(s) = J_0\, \left(1 - \exp\left(-s^2/a^2\right)\right)$. These choices are meant to differentiate between a highly localized secretion at the apex or a slowly decaying secretion away from it. Similarly, for the functional forms of the viscosity, we look at limiting behaviors wherein both a fast and localized increase and a shallower increase are accounted for (Fig. S4 B), keeping fixed the asymptotic form of the divergence in the tubular region.

In Figs. S5 -S9 we plot the results of the numerical integration of the steady-state equations derived in the main text (Eq. 6) using the functional forms of J and μ described above. We see that while the quantitative shape of the pollen tube depends on the choice of these functional forms, the variation of the shape with α does not. In particular, the transition from a non-monotonic curvature κ_s for small values of α to a monotonically decreasing curvature from the apex at large α, is observed in all cases. Importantly, this non-monotonic behavior is obtained with a monotonically decreasing secretion rate and monotonically increasing viscosity. While a detailed comparison with experiments once the

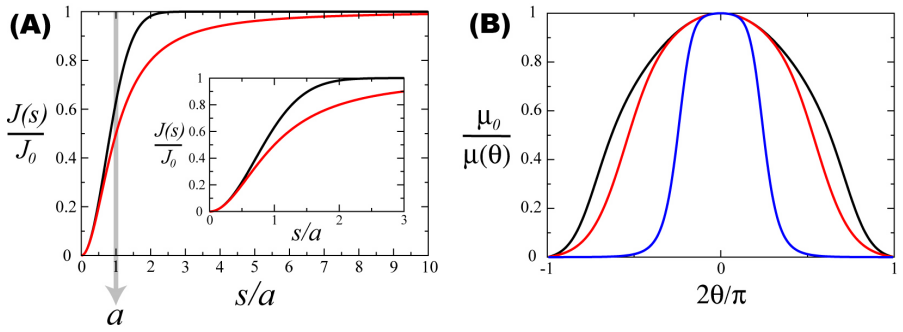

Figure S4: **Spatial dependence of the flux of cell wall material $J(s)$ going through the pollen tube and the wall viscosity $\mu(s)$.** Examples of (A) the flux of cell wall material $J(s)$ and (B) the differential viscosity μ, which have the required asymptotic behaviors. (A) Two functional forms for the flux $J(s)$, associated with slowly and rapidly decaying secretion rates away from the apex were chosen. Slow saturation: $J(s) = J_0\, s^2/(s^2 + a^2)$ (red line). Fast saturation: $J(s) = J_0\, \left(1 - \exp\left(-s^2/a^2\right)\right)$ (black line). The inset shows a close-up of the vicinity of $s = a$, where most of the variation takes place. (B) Three functional forms associated with slowly, moderate and rapidly increasing cell wall viscosity were chosen. The general functional form is $\mu(\theta) = \mu_0\, \left(1 + (c\theta)^d\right) / \cos\theta$, where c and d are dimensionless parameters. A sharp increase of the viscosity corresponds to $c = 2.5$ and $d = 6$ (blue), while shallower increases correspond to $c = 1$ and $d = 6$ (red; corresponds to the functional form used as example in the main text) and for $c = 0.8$ and $d = 10$ (black). We plot the scaled inverse viscosity, i.e. $\mu_0/\mu(\theta)$, for clarity.

functional forms for wall secretion rate and wall rheology is clearly an important goal for the future, the robust qualitative results shown here already allow us to ask comparative questions in the morphology of tip growing cells.

Supplemental References

[1] DoCarmo M (1995) *Differential Geometry of Curves and Surfaces* (Prentice-Hall, N. Jersey).

[2] Landau LD, Lifshitz EM (1986) *Theory of Elasticity* (Butterworth-Heinemann).

[3] Flugge W (1973) *Stresses in Shells* (Springer-Verlag, Berlin).

[4] Batchelor GK (2000) *An Introduction to Fluid Dynamics* (Cambridge University Press).

[5] Vandefliert BW, Howell PD, Ockenden JR (1995) Pressure-driven flow of a thin viscous sheet. *Journal of Fluid Mechanics* 292:359-376.

[6] Bernal R, Rojas ER, Dumais J (2007) The mechanics of tip growth morphogenesis: What we have learned from rubber balloons. *Journal of Mechanics of materials and structures* 2:1157-1168.

[7] Dumais J, Long SR, Shaw SL (2004) The mechanics of surface expansion anisotropy in Medicago truncatula root hairs. *Plant Physiol* 136:3266-75.

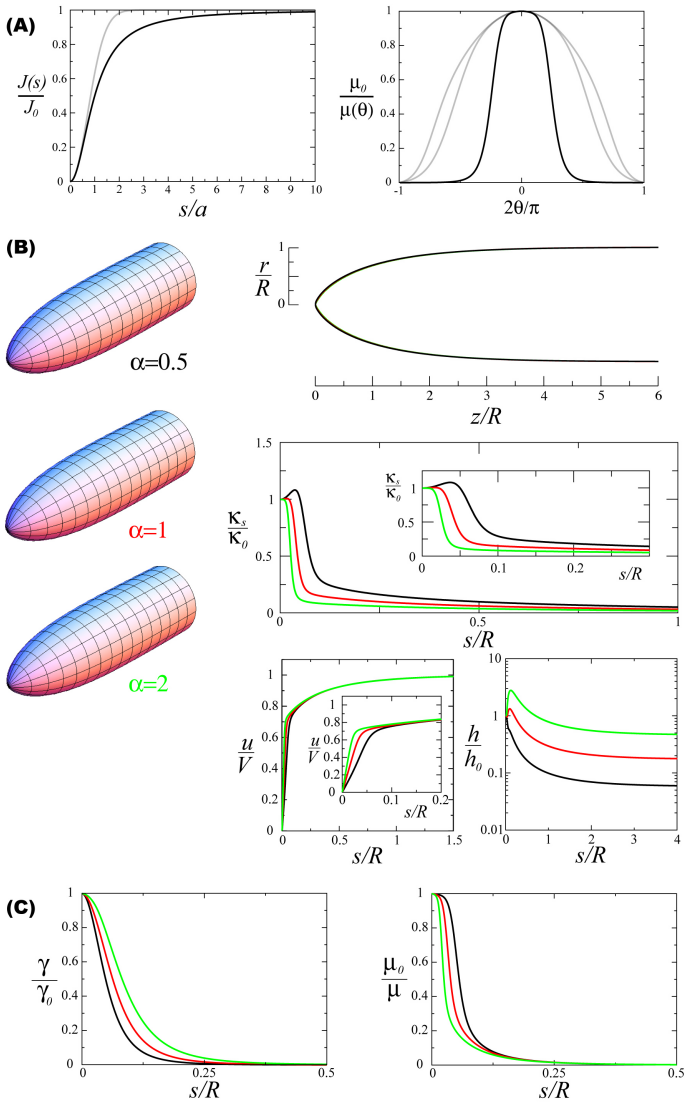

Figure S5: **Numerical solutions of Eq. (6) for a sharp increase in viscosity and slow decay of the secretion rate.** (A) The functional forms $J(s)$ (left) and $\mu(\theta)$ (right) used in the numerical integration are highlighted (black curves) and the other functional forms are shown for comparison (light gray). (B) Pollen tube shapes obtained numerically for different values of the parameter $\alpha \equiv a/R_0$; black - $\alpha = 0.5$, red - $\alpha = 1$, green - $\alpha = 2$. The shapes are also shown in 3D for clarity reasons (left). The curvature $\kappa_s(s)$, the tangential expansion velocity of the cell wall, $u(s)$, and the cell wall thickness, $h(s)$, are shown for the different shapes. The curvature κ_s is non-monotonous for small α and becomes a monotonically decreasing function away from the apex at large α. (C) The scaled secretion rate per unit surface $\gamma(s)$ and scaled inverse viscosity $\mu(s)$ and are plotted as a function of the arclength.

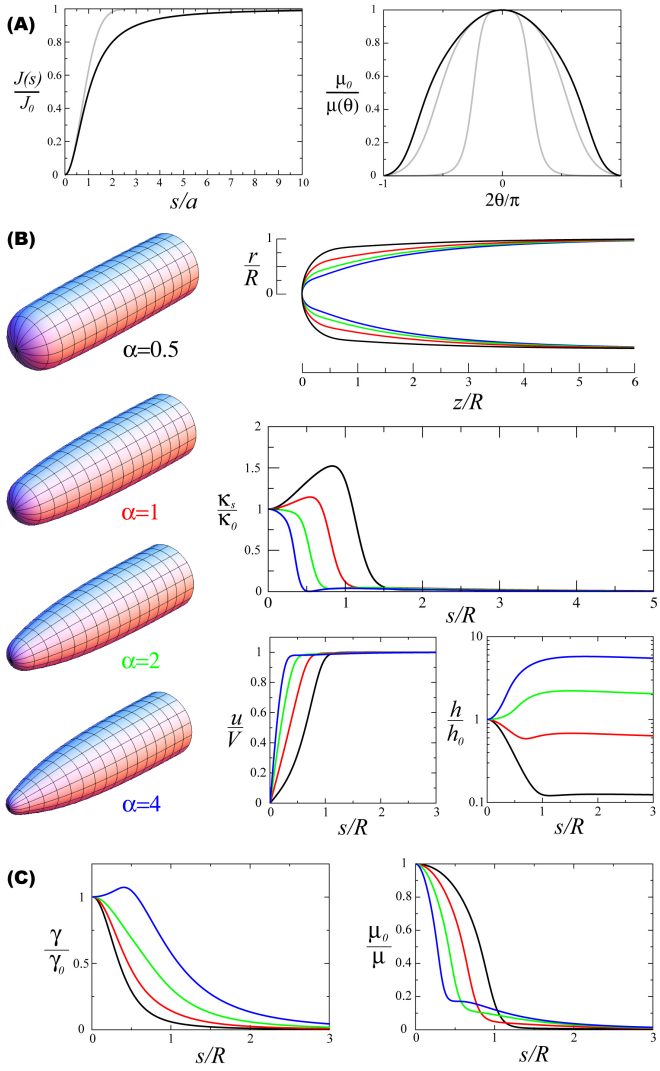

Figure S6: **Numerical solutions Eq. (6) for a very shallow increase in viscosity and slow decay of the secretion rate.** (A) The functional forms $J(s)$ (left) and $\mu(\theta)$ (right) used in the numerical integration are highlighted (black curves) and the other functional forms are shown for comparison (light gray). (B) Pollen tube shapes obtained numerically for different values of the parameter $\alpha \equiv a/R_0$; black - $\alpha = 0.5$, red - $\alpha = 1$, green - $\alpha = 2$, blue - $\alpha = 4$. The shapes are also shown in 3D for clarity reasons (left). The curvature $\kappa_s(s)$, the tangential expansion velocity of the cell wall, $u(s)$, and the cell wall thickness, $h(s)$, are shown for the different shapes. The curvature κ_s is non-monotonous for small α and becomes a monotonically decreasing function away from the apex at large α. (C) The scaled secretion rate per unit surface $\gamma(s)$ and scaled inverse viscosity $\mu(s)$ and are plotted as a function of the arclength. The non-monotonic behavior of the secretion rate γ at large values of α is due to the non-monotonic behavior of the curvature. Note that $J(s)$ is a monotonically increasing function.

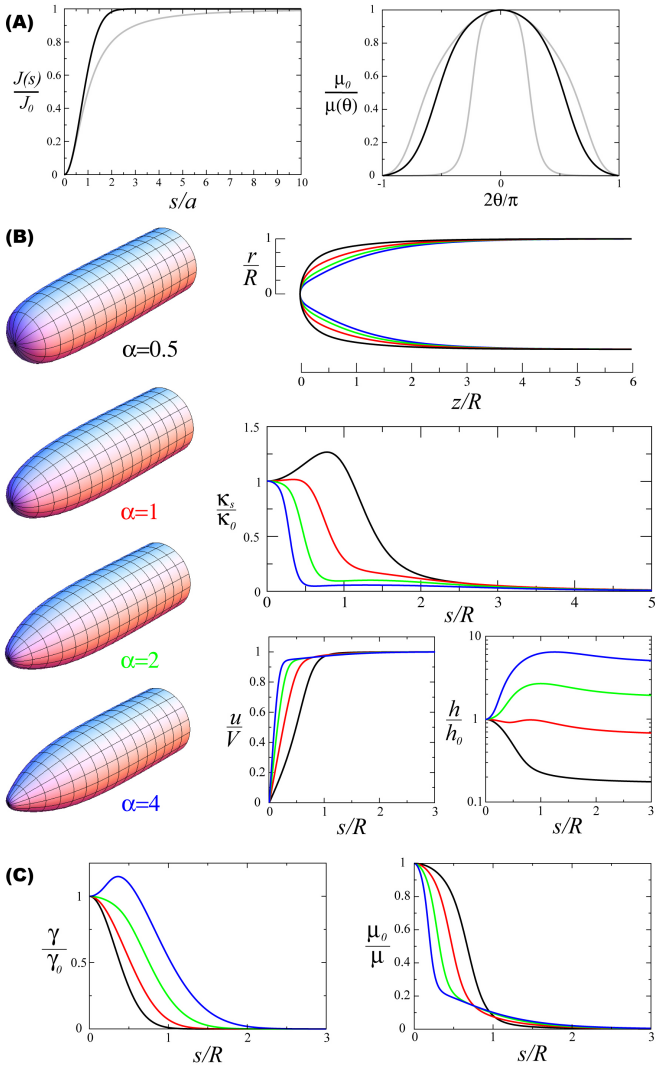

Figure S7: **Numerical solutions Eq. (6) for a shallow increase in viscosity and fast decay of the secretion rate.** (A) The functional forms $J(s)$ (left) and $\mu(\theta)$ (right) used in the numerical integration are highlighted (black curves) and the other functional forms are shown for comparison (light gray). (B) Pollen tube shapes obtained numerically for different values of the parameter $\alpha \equiv a/R_0$; black - $\alpha = 0.5$, red - $\alpha = 1$, green - $\alpha = 2$, blue - $\alpha = 4$. The shapes are also shown in 3D for clarity reasons (left). The curvature $\kappa_s(s)$, the tangential expansion velocity of the cell wall, $u(s)$, and the cell wall thickness, $h(s)$, are shown for the different shapes. The curvature κ_s is non-monotonous for small α and becomes a monotonically decreasing function away from the apex at large α. (C) The scaled secretion rate per unit surface $\gamma(s)$ and scaled inverse viscosity $\mu(s)$ and are plotted as a function of the arclength. The non-monotonic behavior of the secretion rate γ at large values of α is due to the non-monotonic behavior of the curvature. Note that $J(s)$ is a monotonically increasing function.

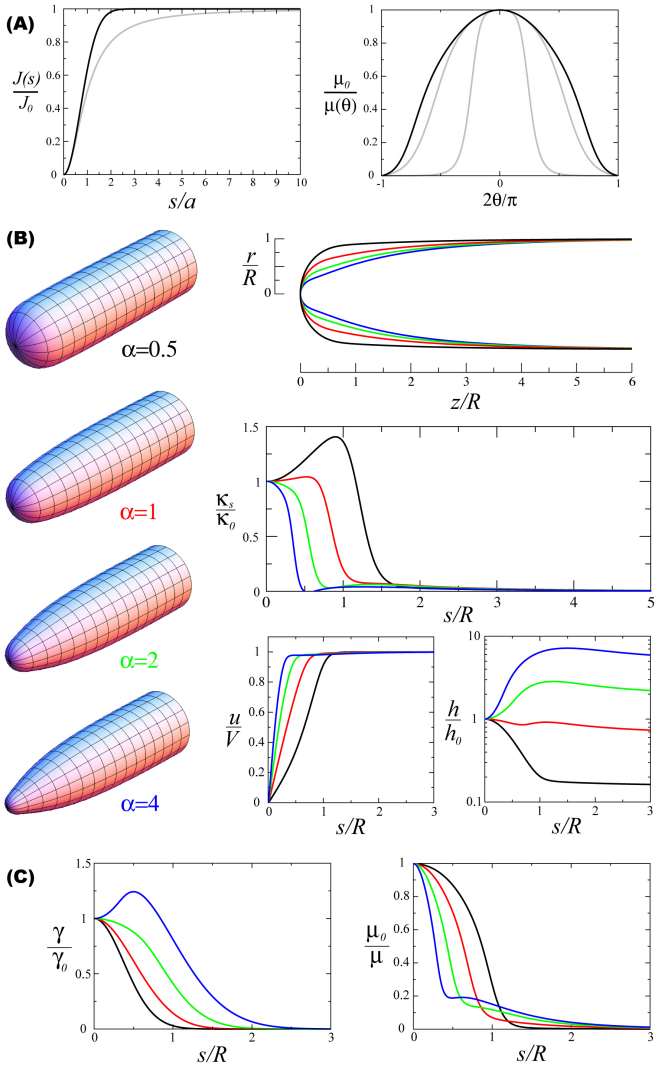

Figure S 8: **Numerical solutions Eq. (6) for a very shallow increase in viscosity and fast decay of the secretion rate.** (A) The functional forms $J(s)$ (left) and $\mu(\theta)$ (right) used in the numerical integration are highlighted (black curves) and the other functional forms are shown for comparison (light gray). (B) Pollen tube shapes obtained numerically for different values of the parameter $\alpha \equiv a/R_0$; black - $\alpha = 0.5$, red - $\alpha = 1$, green - $\alpha = 2$, blue - $\alpha = 4$. The shapes are also shown in 3D for clarity reasons (left). The curvature $\kappa_s(s)$, the tangential expansion velocity of the cell wall, $u(s)$, and the cell wall thickness, $h(s)$, are shown for the different shapes. The curvature κ_s is non-monotonous for small α and becomes a monotonically decreasing function away from the apex at large α. (C) The scaled secretion rate per unit surface $\gamma(s)$ and scaled inverse viscosity $\mu(s)$ and are plotted as a function of the arclength. The non-monotonic behavior of the secretion rate γ at large values of α is due to the non-monotonic behavior of the curvature. Note that $J(s)$ is a monotonically increasing function.

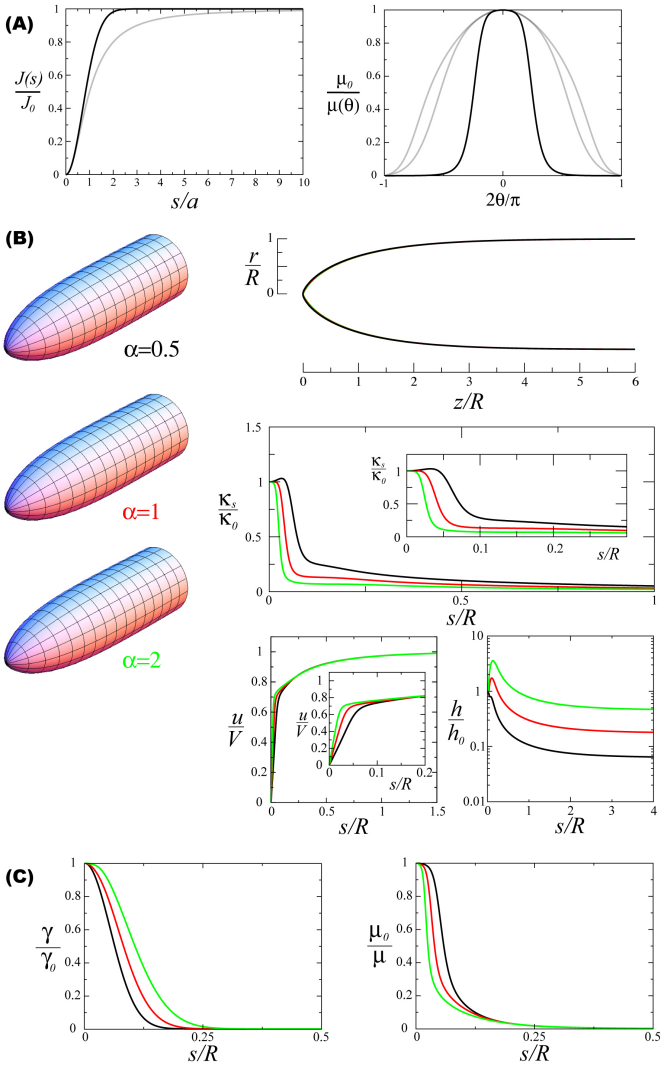

Figure S9: **Numerical solutions Eq. (6) for a sharp increase in viscosity and fast decay of the secretion rate.** (A) The functional forms $J(s)$ (left) and $\mu(\theta)$ (right) used in the numerical integration are highlighted (black curves) and the other functional forms are shown for comparison (light gray). (B) Pollen tube shapes obtained numerically for different values of the parameter $\alpha \equiv a/R_0$; black - $\alpha = 0.5$, red - $\alpha = 1$, green - $\alpha = 2$. The shapes are also shown in 3D for clarity reasons (left). The curvature $\kappa_s(s)$, the tangential expansion velocity of the cell wall, $u(s)$, and the cell wall thickness, $h(s)$, are shown for the different shapes. The curvature κ_s is non-monotonous for small α and becomes a monotonically decreasing function away from the apex at large α. (C) The scaled secretion rate per unit surface $\gamma(s)$ and scaled inverse viscosity $\mu(s)$ and are plotted as a function of the arclength.